PROTEINS: Structure, Function, and Bioinformatics 64:486–501 (2006)

Role of Lysine Versus Arginine in Enzyme Cold-Adaptation: Modifying Lysine to Homo-Arginine Stabilizes the Cold-Adapted α-Amylase from *Pseudoalteramonas haloplanktis*

Khawar Sohail Siddiqui,[1] Anne Poljak,[2] Michael Guilhaus,[2] Davide De Francisci,[1] Paul M. G. Curmi,[3,4] Georges Feller,[5] Salvino D'Amico,[5] Charles Gerday,[5] Vladimir N. Uversky,[6,7,8] Ricardo Cavicchioli[1]*

[1]*School of Biotechnology and Biomolecular Sciences, The University of New South Wales, Sydney, NSW, Australia*
[2]*Bioanalytical Mass Spectrometry Facility, The University of New South Wales, Sydney, NSW, Australia*
[3]*School of Physics, The University of New South Wales, Sydney, NSW, Australia*
[4]*Centre for Immunology, St. Vincent's Hospital, Sydney, NSW, Australia*
[5]*Laboratory of Biochemistry, University of Liege, Institute of Chemistry, Liege-Sart Tilman, Belgium*
[6]*Department of Biochemistry and Molecular Biology, Indiana University, School of Medicine, Indianapolis, Indiana*
[7]*Institute for Biological Instrumentation, Russian Academy of Sciences, Pushchino, Moscow Region, Russia*
[8]*Molecular Kinetics, Indianapolis, Indiana*

ABSTRACT **The cold-adapted α-amylase from *Pseudoalteromonas haloplanktis* (AHA) is a multidomain enzyme capable of reversible unfolding. Cold-adapted proteins, including AHA, have been predicted to be structurally flexible and conformationally unstable as a consequence of a high lysine-to-arginine ratio. In order to examine the role of low arginine content in structural flexibility of AHA, the amino groups of lysine were guanidinated to form homo-arginine (hR), and the structure–function–stability properties of the modified enzyme were analyzed by transverse urea gradient-gel electrophoresis. The extent of modification was monitored by MALDI-TOF-MS, and correlated to changes in activity and stability. Modifying lysine to hR produced a conformationally more stable and less active α-amylase. The k_{cat} of the modified enzyme decreased with a concomitant increase in $\Delta H^{\#}$ and decrease in K_m. To interpret the structural basis of the kinetic and thermodynamic properties, the hR residues were modeled in the AHA X-ray structure and compared to the X-ray structure of a thermostable homolog. The experimental properties of the modified AHA were consistent with K106hR forming an intra-Domain B salt bridge to stabilize the active site and decrease the cooperativity of unfolding. Homo-Arg modification also appeared to alter Ca^{2+} and Cl^- binding in the active site. Our results indicate that replacing lysine with hR generates mesophilic-like characteristics in AHA, and provides support for the importance of lysine residues in promoting enzyme cold adaptation. These data were consistent with computational analyses that show that AHA possesses a compositional bias that favors decreased conformational stability and increased flexibility. Proteins 2006;64:486–501.** © 2006 Wiley-Liss, Inc.

Key words: psychrophilic; guanidination; structure–function–stability relationship; enzyme kinetics; thermodynamics; bioinformatics

INTRODUCTION

Cold-adapted enzymes have been isolated from a broad range of psychrophilic organisms that thrive in permanently cold environments.[1] The primary kinetic adaptation in a psychrophilic enzyme is that its enzyme activity is less temperature dependent (reduced $\Delta H^{\#}$) compared to mesophilic homologues (higher $\Delta H^{\#}$). This is achieved by the enzyme possessing a more flexible structure and as a result, being more thermolabile. Additional features are associated with cold-adapted enzymes, such as high K_m and reduced T_{opt}; however, these characteristics are not present in all psychrophilic enzymes.[1–5] The inherent properties of cold-adapted enzymes has led to their usage in a range of biotechnology applications[3,6–9] and fostered significant interest for determining the structural basis of their high activity and thermolability.[1,3,5]

The α-amylase from the Antarctic bacterium, *Pseudoalteromonas haloplanktis* (AHA) has proven to be a useful enzyme model for studying cold adaptation. The X-ray structure of AHA is most similar to pancreatic porcine α-amylase (PPA).[10] Comparative structural analysis with homologs from mesophiles and thermophiles have shown that cold adaptation in AHA may result from a reduced number of disulfide bridges, an increased number of acidic residues, increased hydrophobic residues on the protein surface, a reduction in proline residues, an increased number of methionine residues, a lower affinity for Ca^{2+}, a decreased number of aromatic interactions, and/or

Abbreviations: AHA, *Pseudoalteromonas haloplanktis* α-amylase; hR, homo-arginine; PPA, pancreatic porcine α-amylase; TFA, trifluroacetic acid; TUG-GE, transverse urea gradient gel electrophoresis.

Grant sponsor: Australian Research Council.

*Correspondence to: Ricardo Cavicchioli, School of Biotechnology and Biomolecular Sciences, The University of New South Wales, Sydney, NSW 2052, Australia. E-mail: r.cavicchioli@unsw.edu.au

Received 13 October 2005; Revised 27 January 2006; Accepted 3 February 2006

Published online 16 May 2006 in Wiley InterScience (www.interscience.wiley.com). DOI: 10.1002/prot.20989

a decrease in the R/R + K ratio.[2,3,11] AHA is a large multidomain enzyme (~ 50 kDa) that is able to unfold reversibly.[12] At moderate temperatures (20–30°C) it unfolds cooperatively by a two-state mechanism.[12–14] However, at 12°C the enzyme unfolds sequentially with two transitions, and at 3°C the structures undergoing first transition show slow interconversions between different conformations.[14] Structures in Domain A in the active site have been shown to form part of the least stable structure of AHA.[14] The low conformational stability and high flexibility of AHA has also been proposed to result from a reduced number of weak ionic interactions in the protein that may facilitate cooperativity and reversible unfolding.[12,15]

Cold-adapted enzymes efficiently catalyze reactions at low temperatures as a result of an inherently high level of flexibility, which provides them with molecular motion sufficient for activity in low energy (cold) environments, and concomitant low conformational stability.[16,17] This relationship between activity, flexibility, and stability represents a central paradigm in the adaptation of proteins to various environments.[18–20] More specifically, the high catalytic activity of psychrophilic enzymes corresponds to the decrease in the magnitude of $\Delta G^{\#}$ for the catalyzed reaction.[2] For all cold-active enzymes, this decrease of $\Delta G^{\#}$ is believed to be achieved by the decrease in $\Delta H^{\#}$ that makes the catalyzed reaction less temperature sensitive, but requires a more flexible active site.[2] The increased flexibility of the structural elements forming the active site (*localized flexibility*) together with the weak overall conformational stability of cold-active enzymes (*global flexibility*) represents the molecular basis for the characteristic heat lability of psychrophilic enzymes.[1,2]

Recently, the effect of amino acid composition on protein flexibility and intrinsic protein disorder has been examined in a broad range of proteins.[21–29] Statistical analyses of amino acid composition, flexibility, hydropathy, charge, coordination number, and several other factors have revealed that sequences of intrinsically disordered (and thus highly flexible) proteins, or regions of proteins, are significantly different from intrinsically ordered (regions of) proteins.[23,30,31] An intrinsically disordered region is characterized by low sequence complexity coupled with a compositional bias; a low content of order-promoting residues, such as bulky hydrophobic amino acids (V, L, I, M, F, W, and Y) which normally form the core of a folded globular protein, and cysteine, and a high proportion of specific polar and charged amino acids (Q, S, P, E, K, and less often, G and A) which promote disorder.[32,33] Interest in this stems from the fact that the inherently flexible regions are often crucial for protein function, and a number of computational tools have been developed for predicting natively disordered regions of proteins.[28,34,35]

In this context it is noteworthy that although high flexibility correlates with low conformational stability (as described above), the relationship between flexibility and intrinsic disorder in proteins has not been well studied. Some proteins have multiple stable states rather than being dynamically disordered (established by X-ray, NMR, and catalytic activity analysis).[36] Proteins may also have relatively rigid overall structures with an increase in the dynamics and flexibility of specific regions, while other proteins may be intrinsically disordered, lacking any rigid ordered structure and displaying a highly dynamic ensemble of rapidly interconverting structures. Irrespective of the nature of protein flexibility, prediction of disorder can help to guide experimental studies.[36] Recently, long disordered segments were successfully predicted in the linker region that separates catalytic and cellulose binding domains in a cellulase from *P. haloplanktis*.[37]

Some of the specific structural features that are predicted to influence the activity/stability of AHA have been experimentally examined using site-directed mutagenesis[13,38] and chemical modification.[39] For example, consistent with a reduced number of disulfide bridges in AHA contributing to its decreased stability, the introduction of a fifth disulfide bridge in a site-directed mutant of AHA resulted in increased conformational stability and reduction in activity.[4,40] By chemically modifying cysteine residues (carboxymethylation) in AHA, it has also been shown that the four native disulfide bridges in AHA appear to promote a localized destabilization (rather than stabilization) of the active site to preserve activity.[39]

Arginine residues are thought to enhance enzyme thermostability more than lysine residues by facilitating more ionic (two salt bridges and five H bond) interactions through their guanidino group.[13,41–43] In a comparative genomics study that used genome sequences of *Archaea*, protein models generated from cold-adapted archaea were found to have fewer charged residues (R + K + E) on their solvent accessible surface.[44] Experimental support for the thermostabilizing effect of arginine over lysine comes from studies on a range of mammalian enzymes that were reported to be stabilized by the introduction of guanidinium groups.[41] To date, this has not been tested in AHA or any other enzymes from psychrophiles.[5]

AHA has only 13 R and 13 K residues, compared to 28 R and 19 K residues in PPA.[15,45] To assess the role that lysine and arginine play in the thermal stability of AHA, we converted the side-chains of lysine residues to homoarginine (hR) by guanidination of amino groups. The extent of modification over time was quantitated by MALDI-TOF-MS. The effect of modification on the biophysical characteristics of AHA were assessed by transverse urea gradient gel electrophoresis (TUG-GE), far-UV circular dichroism (CD), and proteolytic nicking. A protein homology model with hR replacing K was generated to enable the biophysical experimental data to be placed in a structural context, and several computational tools were used to analyze the amino acid composition of AHA. In addition, computational predictions of disorder in AHA were evaluated in view of our experimental findings. As a result, we were able to assign a critical role for flexibility in the active site to Domain B. This complemented previous work that defined an important role for Domain A in the active site.[14] Our findings are consistent with the presence of lysine at position 106 in unmodified AHA, preventing the formation

of a salt bridge that is otherwise present in more thermostable α-amylases (e.g., R124-E138 in PPA).

MATERIALS AND METHODS

Chemical Modification

The recombinant wild-type AHA and N12R mutant were prepared as described previously.[13] Total protein content was determined by Bradford assay using bovine serum albumin as standard.[46] Guanidination of lysine amino groups to form hR residues was performed as described previously.[47] AHA (1 mg) was suspended in 10 mL solution containing 0.5*M* 3,5-dimethylpyrazole-1-carboxamidine nitrate/NaOH, pH 9.5, 50 m*M* NaCl, and 50 m*M* maltose at 1 to 2°C for 17, 46, or 66 h. The reaction was stopped by dialyzing out reagents against a solution containing 50 m*M* MOPS/NaOH, pH 7.2 and 50 m*M* NaCl at 5°C.

Enzyme Kinetics and Thermodynamics of Activation

Kinetic and thermodynamic analyses at 3°C and 25°C were performed as described previously.[39,48,49]

Transverse Urea Gradient Gel Electrophoresis

TUG-GE was performed and TUG gels analyzed as described previously.[14,49]

Circular Dichroism

The far-ultraviolet (UV; 205–240 nm) CD spectra of unmodified and modified AHA were recorded using a JASCO-Europe J-810CD spectropolarimeter under constant nitrogen flow, connected to a Peltier temperature controller (JASCO-Europe) set at 12°C. Spectra were recorded using a 0.1 cm path length and a protein concentration of 0.33 mg mL^{-1}. All measurements were carried out at 12°C in a solution containing 10 m*M* MOPS, 50 m*M* NaCl, 1 m*M* $CaCl_2$ (pH 7.5) as described previously.[12] Spectra were averaged over 10 scans and corrected for buffer signal. Raw data were expressed in terms of the mean residue ellipticity (θ) using the following parameters: molecular weight, concentration, cell path length, and number of residues.

Proteolytic Nicking

Unmodified and hR-modified (17 h) enzymes were subjected to limited proteolysis using AHA:chymotrypsin ratio of 1:20 (w/w) in 10 m*M* MOPS, 50 m*M* NaCl, 1 m*M* $CaCl_2$, pH 7.5 at 30°C.[50,51] At different time intervals (0, 0.5, 2, and 5 h), the digestion was stopped by the addition of SDS loading buffer,[52] and the samples were immediately boiled for 5 min and electrophoresed by SDS-PAGE.[49] The gel was stained using Coomassie R-250.[52] Gel profiles were scanned using a LAS-3000 (Fujifilm, Berthold, Australia) and the image was analyzed with Image-Gauge 4.0 software. Band intensities of unmodified and modified AHA relative to their respective undigested (0 h) samples were plotted against time.

MALDI-TOF Mass Spectrometry

AHA was cleaved using endolys-C and endoAsp-N proteases and samples prepared for peptide mass mapping. Guanidinated AHA preparations were run on a Coomassie stained one-dimensional SDS polyacrylamide gel (1D-gel) and bands were excised. In-gel enzymatic cleavage, using endolys-C and endoAsp-N proteases, was performed by a modification of previously published procedures.[39,53] Endolys-C peptides extracted from the gel were captured onto C4 ziptips, desalted with four to five washes (20 μL each) with acetonitrile:TFA:water (2:0.1:98 v/v/v) and eluted directly onto a stainless-steel MALDI target in caffeic acid matrix (10 mg/mL in acetonitrile:TFA:water 80:0.1:20 v/v/v) in a total volume of 1.5 μL. EndoAsp-N peptides were extracted using C18 Sep Pak solid phase extraction cartridges, washing with acetonitrile:TFA:water (2:0.1:98 v/v/v) and eluting with 1.5 μL acetonitrile:water:TFA (80:20:0.1 v/v/v). Samples were dried under reduced pressure and redissolved in 50 μL acetonitrile:water:TFA (80:20:0.1 v/v/v). Samples (0.1 μL) were directly applied to the MALDI target, together with 0.5 μL matrix (10 mg/mL) of either dihydroxybenzoic acid or α-cyano-4-hydroxycinnamic acid in acetonitrile:water:TFA; 80:20:0.1 v/v/v).

All of the MALDI analyses were performed on a Voyager DE STR mass spectrometer with a nitrogen laser (337 nm; 2 ns pulse) from PE Biosystems (Framingham, MA). Data acquisition was performed in the positive ion mode and the instrument was calibrated immediately prior to each analysis. Three-point external calibration was performed using calmix 1 from the Sequazyme kit and mono-isotopic masses of the singly protonated molecular ions of des-Arg-Bradykinin [$(M + H)^+ = 904.47$], Angiotensin 1 [$(M + H)^+ = 1296.69$], and Glu-Fibrinopeptide B [$(M + H)^+ = 1570.68$] were used to calibrate the mass axis. All analyses were initially performed in reflectron delayed extraction mode. However in the case of the Endolys-C digests of modified AHA some peptides > 10k Da were anticipated, so these samples were also analyzed using caffeic acid matrix in linear delayed extraction mode. Analyses using two matrices also enabled the optimization of the number of peptides detected in order to maximize sequence coverage. Once applied to the MALDI target all samples were air dried at ambient temperature prior to analysis. PAWS software[54] was used to facilitate identification of peptide masses observed in the spectra. Following Asp-N proteolysis, the 13 K residues in AHA appear in unique Asp-N peptides, with the exception of K_{443} and K_{446} which both appear in peptide 437 to 448. Modified and unmodified peptide peaks which both appear in the spectra were integrated to provide peak areas from which relative levels of modification were obtained. The Voyager Data Explorer software was used to integrate peak areas and levels of modified and unmodified lysine containing peptides were estimated as a percentage of the summed areas. The accuracy of this method is predicated on the relative ionization efficiency of guanidinated and nonguanidinated peptides being essentially identical. A similar approach was used in a previous study.[55]

Computational Methods

Potential new interactions (H bonds and salt bridges) formed as a result of the conversion of amino groups of K

TABLE I. MALDI-TOF Analysis of Unmodified and hR-Modified AHA Following Endo-lysC Proteolysis

Peptide Sequence[a]	Theoretical Mass[b]	Observed Mass[b] Unmodified AHA	Observed Mass[b] hR, 17 h	K Residues[c] hR, 17h Unmodified K	Observed Mass[b] hR, 46h	K Residues[c] hR, 46h Unmodified K
1–27	3325.7	3326.6	3326.2	K_{27}	3327.8	K_{27}
28–106	8535.4	8536.9	8536.1	K_{27}, K_{106}		
107–169	7160.8	7163.5	7162.6	K_{106}, K_{169}		
170–177	928.0	928.1	927.8	K_{169}, K_{177}		
178–190	1371.6	1371.6				
191–224	3528.9	3529.4				
225–300	8385.2	8386	8384.5	K_{224}, K_{300}		
301–334	3739.0	3740.5	3740.3	K_{300}, K_{334}		
335–383	5658.1	5658.9	5657.9	K_{334}, K_{383}		
384–406	2533.8	2534.6				
384–414	3305.6	3309.6				
415–443	3075.4	3076.5	3075.9	K_{414}, K_{443}		
				Modified K[d]		Modified K[d]
1–169 + hR ×3	19111.8				19109.6	N-terminus, K_{27}, K_{106}
1–190 + hR ×5	21457.4				21459.7	N-terminus, K_{27}, K_{106}, K_{169}, K_{177}
170–190 + hR ×1	2322.6		2322.7	K_{177}		
170–224 + hR ×2	5874.5		5873.6	K_{177}, K_{190}		
178–224 + hR ×1	4923.5		4923.7	K_{190}		
191–300 + hR ×1	11938.1				11945.1	K_{224}
384–414 + hR ×1	3347.6		3349.9	K_{406}	3349.8	K_{406}
407–443 + hR ×1	3889.3		3890.0	K_{414}	3890.6	K_{414}
407–446 + hR ×2	4244.6		4244.9	K_{414}, K_{443}	4247.3	K_{414}, K_{443}
415–446 + hR ×1	3430.8		3431.4	K_{443}	3432.8	K_{443}
Sequence Coverage		98.9%	99.6%		81%	

[a]hR denotes the number of K residues guanidinated in that peptide. Modified lysines (hR) are not cleaved by endo-LysC.
[b]All values are average masses and expressed as the singly protonated molecular ion represented by $[M+H]^+$.
[c]Unmodified K residues inferred from comparison of the theoretical and observed data for 17 h and 46h hR-modified AHA.
[d]Modified K residues inferred from comparison of the theoretical and observed data for 17 h and 46h hR-modified AHA.

TABLE II. MALDI-TOF Analysis of Unmodified and hR-Modified AHA Following Endo-aspN Proteolysis

Peptide Sequence	Lysine Residue	Theoretical Mass[a]	Observed Mass[a] Unmodified AHA	Observed Mass[a] hR, 17 h	% Peak Area[b] hR, 17 h	Observed Mass[a,b] hR, 46 h	% Peak Area[b] hR, 46 h	Observed Mass[a,b] hR, 66 h	% Peak Area[b] hR, 66 h
84–114	K_{106}	3140.5	3140.3	3141.7	11.0%	3140.1	2.6%	BLD	0%
84–114	**K_{106}**	**3182.5**		**3183.8**	**89.0%**	**3183.8**	**97.4%**	**3184.0**	**100%**
162–173	K_{169}	1350.7	1350.6	1350.8	35.5%	1350.9	8.2%	1350.9	3.8%
162–173	**K_{169}**	**1392.7**		**1392.8**	**64.5%**	**1392.9**	**91.8%**	**1393.0**	**96.2%**
174–182	K_{177}	885.4	885.5	885.5	20.9%	885.5	10.8%	BLD	0%
174–182	**K_{177}**	**927.4**		**927.5**	**79.1%**	**927.5**	**89.2%**	**927.6**	**100%**
183–202	K_{190}	2174.1	2174	2174.3	4.1%	2174.2	2.2%	2173.7	0.4%
183–202	**K_{190}**	**2216.1**		**2216.3**	**95.9%**	**2216.4**	**97.8%**	**2216.5**	**99.6%**
285–305	K_{300}	2429.1	2428.9	2429.3	5.2%	BLD	0%	BLD	0%
285–305	**K_{300}**	**2471.1**		**2471.4**	**94.8%**	**2471.4**	**100%**	**2471.6**	**100%**
312–346	K_{334}	3914.7	3916.3	3916.0	67.7%	3918.0	2.0%	3917.5	0.9%
312–346	**K_{334}**	**3956.7**		**3958.7**	**51.9%**	**3959.3**	**98.0%**	**3958.7**	**99.1%**
363–384	K_{383}	2377.1	2376.9	2377.2	33.8%	2378.0	2.7%	2379.6	0.9%
363–384	**K_{383}**	**2419.1**		**2419.3**	**66.2%**	**2419.4**	**97.3%**	**2419.4**	**99.1%**
395–411	K_{406}	1843.8	1843.6	1843.9	65.3%	1844.0	71.5%	1844.1	35.8%
395–411	**K_{406}**	**1885.8**		**1886.0**	**34.7%**	**1886.1**	**28.5%**	**1886.1**	**64.2%**
412–425	K_{414}	1467.7	1467.7	1467.7	21.1%	1467.7	11.4%	BLD	0%
412–425	**K_{414}**	**1509.7**		**1509.8**	**78.9%**	**1509.8**	**88.6%**	**1509.9**	**100%**

[a]All values are monoisotopic masses and expressed as the singly protonated molecular ion represented by $[M+H]^+$.
[b][(peak area modified)/(peak area unmodified + peak area modified)] × 100.
Quantification was not possible for unmodified peptide 15–68 and modified peptide 203–260 as their peak masses overlap.
Peptide 437–448 does not appear in any of the spectra (either unmodified or modified). BLD, below limit of detection.
Bold indicates modified lysine residues (hR)

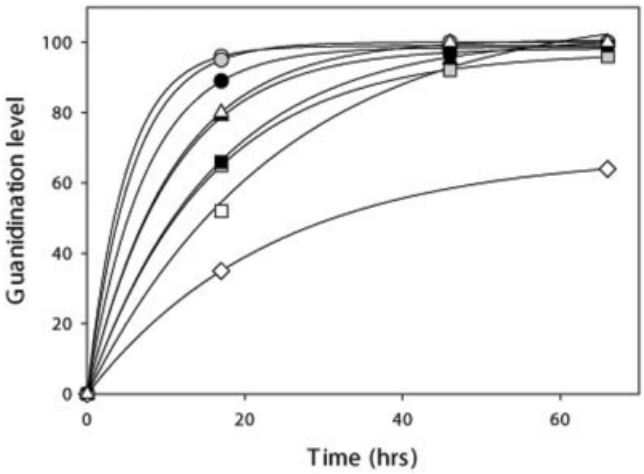

Fig. 1. Kinetics of guanidination of lysine resides. K106 (black circles), K169 (gray squares), K177 (black triangles), K190 (open circles), K300 (gray circles), K334 (open squares), K383 (black squares), K406 (open diamonds), and K414 (open triangles).

residues into guanidinium side-chains of hR were assessed by visual inspection using program O.[56] A guanidium group was visually docked onto K residues in the crystal structure (PDB: 1AQM) without changing the rotamer observed. Primary sequence alignments of AHA with α-amylases from mammals were constructed using T-COFFEE.[57] The prediction of intrinsic disordered regions in AHA and PPA were carried out using FoldIndex[58] based on the mean net charge and mean hydrophobicities of a protein.[59] The distribution of the propensity for intrinsic disorder in the AHA sequence was analyzed using the PONDR® VL-XT algorithm.[30,32,35] Access to PONDR® was through Molecular Kinetics (http://www.molecularkinetics.com).

RESULTS

Identification of Modified Lysine Residues

The K residues of AHA were chemically modified by guanidination. A single chemically modified enzyme provides a global view of the impact of simultaneously modifying all 13 K residues in AHA. This is one of the mildest forms of chemical modification as no bulky groups are introduced and the charge profile of the enzyme is not altered.[47] In order to follow the extent of guanidination over time, modified and unmodified AHA was digested with endoLys-C (Table I) or endoAsp-N (Table II) proteases and analyzed by MALDI-TOF-MS mass mapping.

Conversion of K to hR renders the modified amino acid resistant to endoLys-C cleavage. As a result the length of endoLys-C peptides increase with the extent of modification. MALDI-TOF-MS mass mapping of endoLys-C cleaved AHA achieved 98.9% sequence coverage for unmodified AHA and 81% to 99.6% coverage for the modified forms of AHA (Table I). The high level of sequence coverage was facilitated by the small number of AHA peptides generated by endoLys-C cleavage (14 theoretical peptides). However, the large number of peptide mass variants generated as a result of differential guanidination of the 13 K residues, limited the ability to detect all peptides. Following 17 h

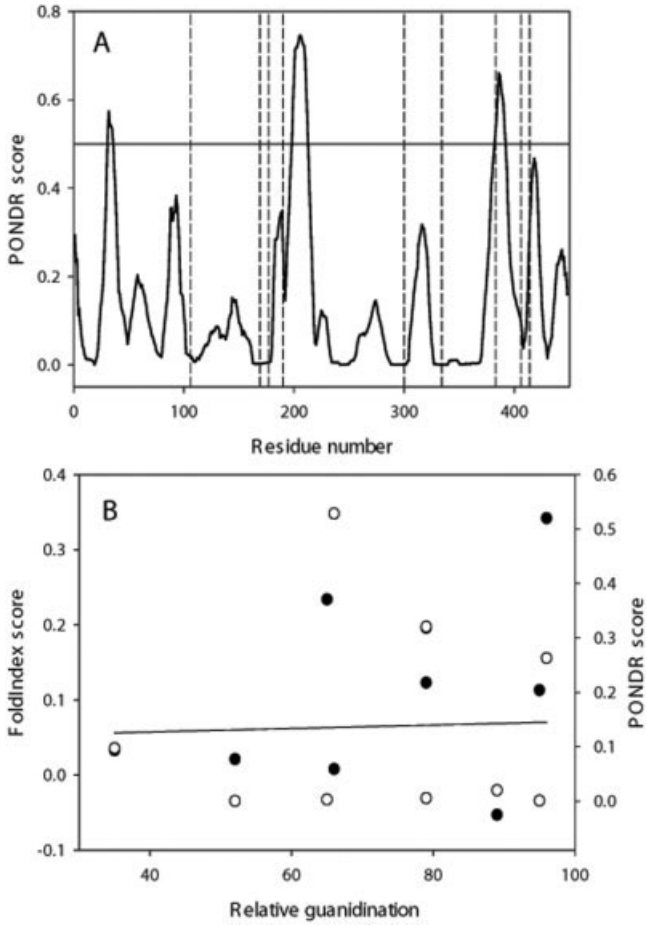

Fig. 2. Analysis of the correlation between the intrinsic disorder and efficiency of guanidination. (**A**) PONDRing AHA. Distribution of PONDR® score within the AHA sequence. Higher scores correspond to more flexible regions. PONDR® score above 0.5 is characteristic of the intrinsically disordered region. Positions of K106, K169, K177, K190, K300, K334, K383, K406, and K414 are indicated by vertical dashed lines. Black and gray bars correspond to α-helices and long β-strands; localization of which was determined from the crystal structure of the protein (PDB accession number for AHA is 1AQM). (**B**) Dependence of the guanidination efficiency (estimated for each lysine as relative amount of modified residue after 17 h guanidination) on FoldIndex (black circles) and PONDR® VL-XT scores (open circles). Straight line corresponds to the best linear fit.

guanidination, 10 of the K residues were partially modified and 5 (K177, K190, K406, K414, and K443) were completely guanidinated. After 46 h guanidination, only K27 remained partially unmodified whereas eight residues were fully guanidinated. The guanidination reagent reacts very slowly with N-terminal amino acids[47] and therefore this amino acid was only partially modified after 46 h.

EndoAsp-N cleaves at the N-terminal side of D residues and was used to generate peptides containing modified or unmodified K residues to enable a semiquantitative estimation of the extent of modification using MALDI-TOF-MS (Table II). Between 63% to 86% sequence coverage was achieved for all preparations and qualitative data was obtained for 11 of the 13 K residues present in AHA. No signal was obtained for peptide 437 to 448, which contains two K residues. The majority of K residues were suscep-

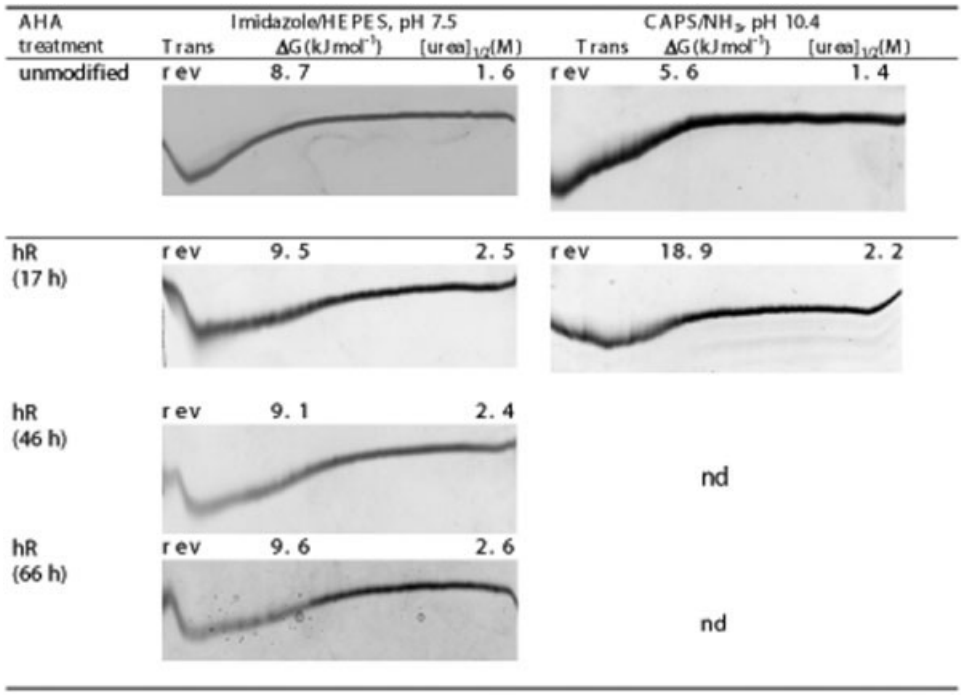

Fig. 3. Urea unfolding curves and thermodynamic parameters of unmodified and modified AHA in the presence of calcium at 30° C. TUG-GE performed at pH 7.5 and 10.4 in the presence of Ca^{2+} at 30°C. Urea gradient was 0 to 6.64*M* (left to right); direction of electrophoresis, top to bottom; nd, not determined; Trans, folding/unfolding transition; rev, reversible transition; ΔG, free energy of unfolding between transitions; $(urea)_{1/2}$, urea concentration at 0 ΔG.

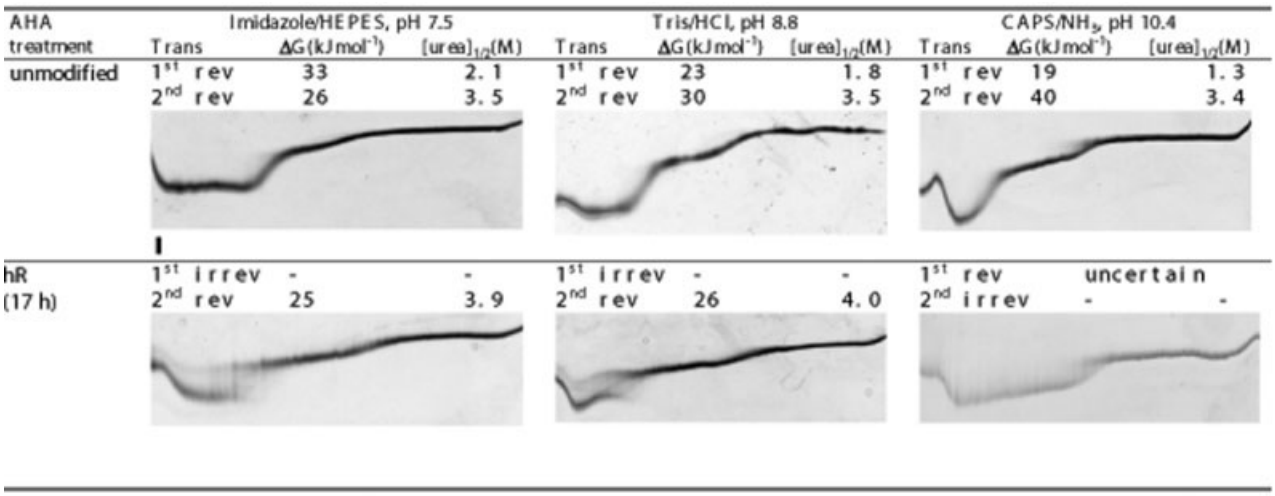

Fig. 4. Urea unfolding curves and thermodynamic parameters of unmodified and modified AHA in the presence of calcium at 12°C. TUG-GE performed at pH 7.5, 8.8, and 10.4 in the presence of Ca^{2+} at 12°C. Urea gradient was 0 to 6.64*M* (left to right); direction of electrophoresis, top to bottom; Trans, first or second folding/unfolding transition; rev, reversible transition; ΔG, free energy of unfolding between transitions; $(urea)_{1/2}$, urea concentration at 0 ΔG.

tible to guanidination at 17 h, however no assessment of K224 could be made as the peak masses of unmodified peptide 15 to 68 and guanidinated peptide 203 to 260 overlap. The 6200 mass is likely to contain a mixture of both. However, the majority is probably peptide 15 to 68 because in the spectrum of the unmodified protein the peak intensity for this peptide is much greater than for peptide 203 to 260.

To quantify the extent of guanidination of K residues over the 17 to 66 h modification period, the peak areas of unmodified and guanidinated peptides were integrated and the relative percentage of each calculated (Table II), and the kinetics of guanidination plotted for K106, K169, K177, K190, K300, K334, K383, K406, and K414 (Fig. 1). Semiquantitative data were obtained for 9 K residues. The majority of these nine lysines were > 50% guanidinated at

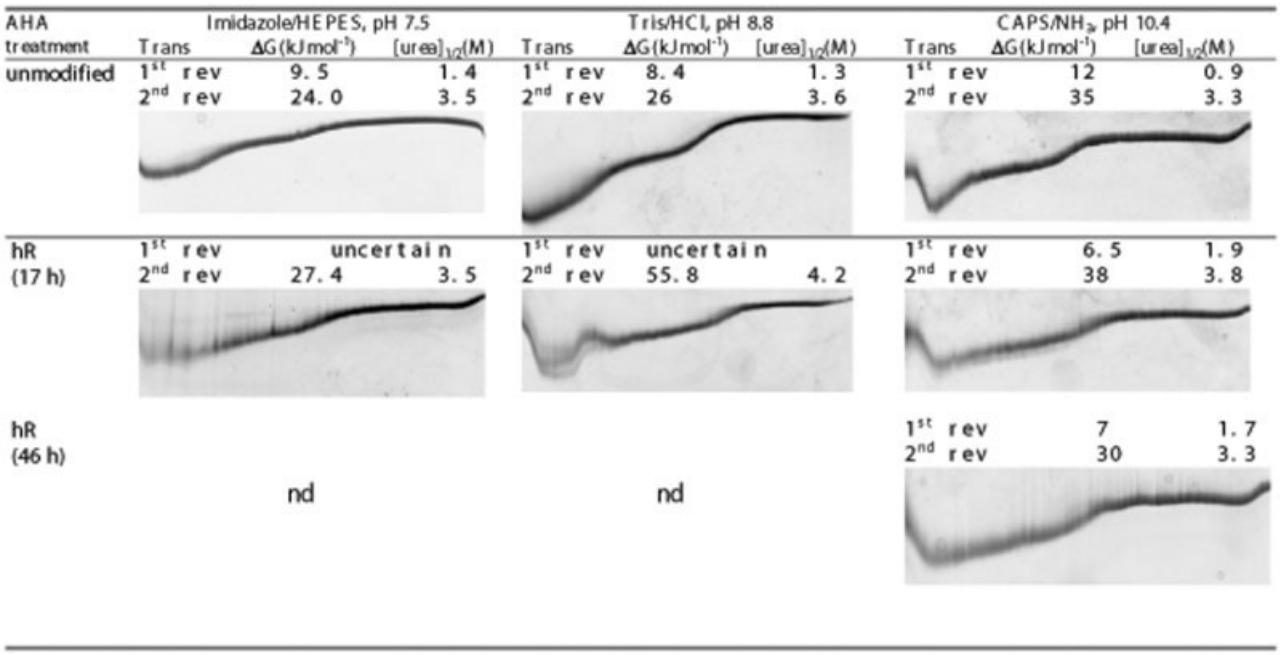

Fig. 5. Urea unfolding curves and thermodynamic parameters of unmodified and modified AHA in the presence of EDTA at 12°C. TUG-GE performed at pH 7.5, 8.8, and 10.4 in the absence of Ca^{2+} (presence of EDTA) at 12°C. Urea gradient was 0 to 6.64*M* (left to right); direction of electrophoresis, top to bottom; nd, not determined; Trans, first or second folding/unfolding transition; rev, reversible transition; ΔG, free energy of unfolding between transitions; $(urea)_{1/2}$, urea concentration at 0 ΔG.

17 h, 90% to 100% at 46 h, and essentially fully modified by 66 h. The least reactive K residue was K406, which was 35% modified after 17 h and 64% after 66 h. The K residues closest to the C-terminus (K334, K383, K406, and K414) were the slowest to guanidinate (35%–79% at 17 h), followed by those towards the N-terminus (K106, K169, and K177), which were 65% to 89% at 17 h. The fastest reacting groups were K190 and K300, which were 95% guanidinated at 17 h.

To understand the potential role that flexibility (i.e., predisposition for intrinsic disorder) plays in affecting the efficiency of guanidination, the extent of modification of the nine K residues (K106, K169, K177, K190, K300, K334, K383, K406, and K414) following 17 h guanidination was plotted against the disorder score from PONDR® VL-XT [Fig. 2(A)] and FoldIndex [Fig. 2(B)] analyses. The distribution of the major secondary structure elements, α-helices (black bars) and long β-strands (gray bars), within the AHA sequence is shown in Figure 2(A). There is a good overall agreement between the distribution of intrinsic disorder and experimentally determined localization of secondary structure elements. The vast majority of stable secondary structure elements (α-helices and β-strands) are located within regions with low disorder scores, whereas regions with high predicted disorder mostly coincide with loops (more flexible structural elements). This finding shows that the shape of the PONDR VL-XT curve might reflect flexibility of ordered proteins and illustrates the value of applying the prediction of intrinsic disorder propensity to explain flexibility. However, data presented in Figure 2 did not reveal a good correlation between the propensity for intrinsic disorder and the efficiency of guanidination. For example, K300 is one of the fastest reacting groups (Fig. 1) and is located within a region that is strongly predicted to be ordered, whereas K383 is one of the slowest reacting groups (Fig. 1) and is located within a region that is predicted to be disordered [Fig. 2(A)]. This outcome is unexpected in light of previous observations that the sites of proteolysis tend to be located in more flexible regions.[60–62]

The solvent accessible of lysines on the surface of AHA was examined using the Contacts of Structural Units (CSU) software.[63] This revealed that all K residues in AHA are largely buried, with relative solvent accessible surface area ranging from 0.7% to 39.2%. The degree of solvent accessibility could not be correlated to guanidination efficiency. For example, despite its high rate of modification (Fig. 1), the relative solvent accessible surface area of K300 was 0.7%.

Effect of Guanidination on Conformational Stability

TUG-GE is useful for differentiating protein conformations and enables thermodynamic and kinetic properties of transitions between conformational states to be analyzed.[49,64,65] TUG-GE was recently employed to identify intermediate states and to determine which domain unfolds first in the unfolding pathway of AHA.[14]

In order to accurately compare the overall conformational stability of AHA following modification for 17, 46, and 66 h, baseline TUG-GE curves for the fully folded forms of the modified and unmodified enzymes were established, and ΔG and the midpoint of urea unfolding [$(urea)_{1/2}$] were calculated (Fig. 3). A single continuous

TABLE III. Kinetic and Thermodynamic Data of Potato Starch Hydrolysis for Unmodified and hR-Modified AHA at 3 and 25°C

α-Amylases Parameters	Unmodified	hR (17 h)	hR (46 h)	hR (66 h)
T_{opt} (°C)	32	29	32	—
3 °C				
k_{cat} (sec^{-1})	840	66.7	—	—
K_m (mg mL^{-1})	2.3	1.5	—	—
$\Delta G^{\#}$ (kJ mol^{-1})	52	58	—	—
$\Delta H^{\#}$ (kJ mol^{-1})	26	32	—	—
$\Delta S^{\#}$ (J mol^{-1} K^{-1})	−93	−94	—	—
25 ° C				
k_{cat} (sec^{-1})	2321	120	25.5	10
k_m (mg mL^{-1})	2.9	1.3	2.0	3.6
$\Delta G^{\#}$ (kJ mol^{-1})	54	61	65	67
$\Delta H^{\#}$ (kJ mol^{-1})	26	32	42	—
$\Delta S^{\#}$ (J mol^{-1} K^{-1})	−94	−98	−77	—

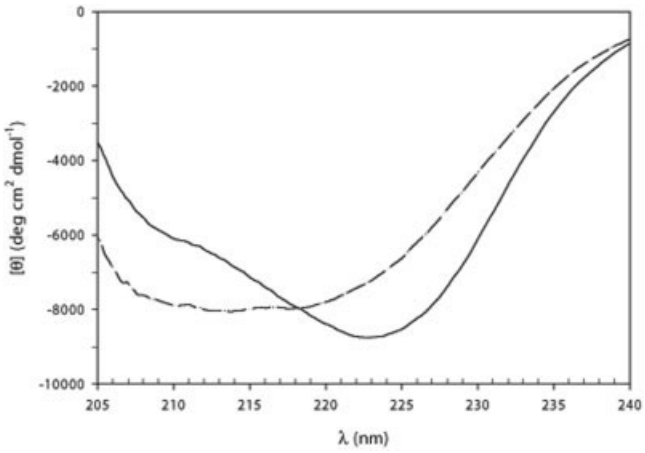

Fig. 6. CD spectra in the far-UV at 12°C. Unmodified (continuous curve) and hR-modified (17 h) (broken curve) AHA.

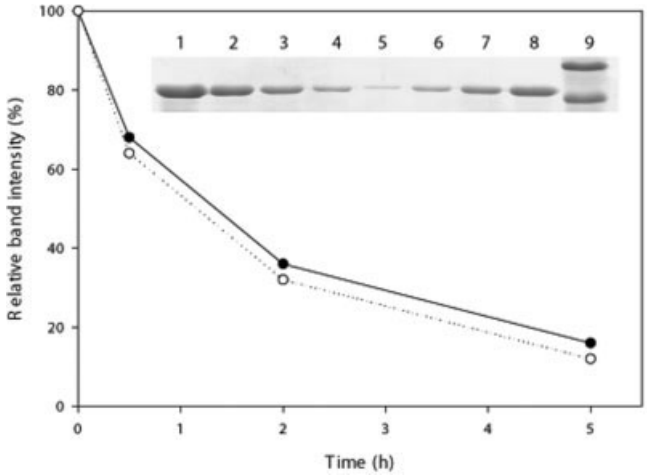

Fig. 7. Rate of digestion of unmodified and modified AHA by chymotrypsin at 30°C. Unmodified AHA, continuous line; modified AHA, dotted line. Inset graph: 12% SDS-PAGE of unmodified and modified AHA samples treated with chymotrypsin for various times. Lanes 1 to 4, unmodified AHA after 0, 0.5, 2, and 5 h incubation in the presence of chymotrypsin, respectively. Lanes 8 to 5, modified AHA after 0, 0.5, 2, and 5 h incubation in the presence of chymotrypsin, respectively. Lane 9, molecular weight markers (upper band, 66 kDa; lower band, 45 kDa).

transition was observed when TUG-GE was performed at 30°C, under varying conditions of pH and presence or absence of Ca^{2+} (Fig. 3). TUG-GE patterns were superimposable when the folded enzyme (N⇆U) and the unfolded enzyme preincubated in 6.64*M* urea (U⇆N) were run under parallel conditions (data not shown). This response is typical for an enzyme that unfolds/folds reversibly[64,65] and was previously demonstrated for AHA.[14]

In imidazole-HEPES (pH 7.5), Ca^{2+} buffer, the $(urea)_{1/2}$ (2.4–2.6*M*) and ΔG (9.1–9.6 kJ mol^{-1}) of modified AHA (17, 46, and 66 h) was higher than for unmodified AHA [$(urea)_{1/2}$, 1.6*M*; ΔG, 8.7 kJ mol^{-1}; Fig. 3]. In CAPS-NH_3 (pH 10.4), Ca^{2+} 17 h modification led to an increase of 13 kJ mol^{-1} in ΔG and 0.8*M* in $(urea)_{1/2}$ (Fig. 3). These data demonstrate that guanidination improved the stability at both neutral and alkaline pH. The TUG-GE analysis also showed that conformational stability of the modified enzyme (17 h) was more pronounced at pH 10.4 compared to pH 7.5 (18.9 kJ mol^{-1} vs. 9.5 kJ mol^{-1}) and compared to the unmodified enzyme (5.6 kJ mol^{-1} vs. 8.7 kJ mol^{-1}), indicating that guanidination made the enzyme increasingly more alkali stable. The pK_a of guanidino groups (12.5) in hR residues is higher than the amino group (10.5) in K residues. As a result, guanidino groups will remain positively charged at high pH and salt bridges will have more opportunity to form.

Effect of Guanidination on Unfolding Cooperativity

TUG-GE of modified and unmodified AHA was performed at 12°C in the absence or presence of Ca^{2+} to examine the effect of guanidination on unfolding cooperativity. In the presence of Ca^{2+} at pH 7.5 and 8.8, the unmodified enzyme unfolded reversibly with two transitions (Fig. 4). In contrast, TUG-GE of the modified enzyme (17 h) revealed a break in the unfolding curve at low urea concentrations, demonstrating that the first transition corresponds to a slow unfolding process; that is, the time taken to unfold is greater than the duration of electrophoresis (Fig. 4). These data show that in contrast to fast unfolding at 30°C in the presence of Ca^{2+} (Fig. 3), unfold-

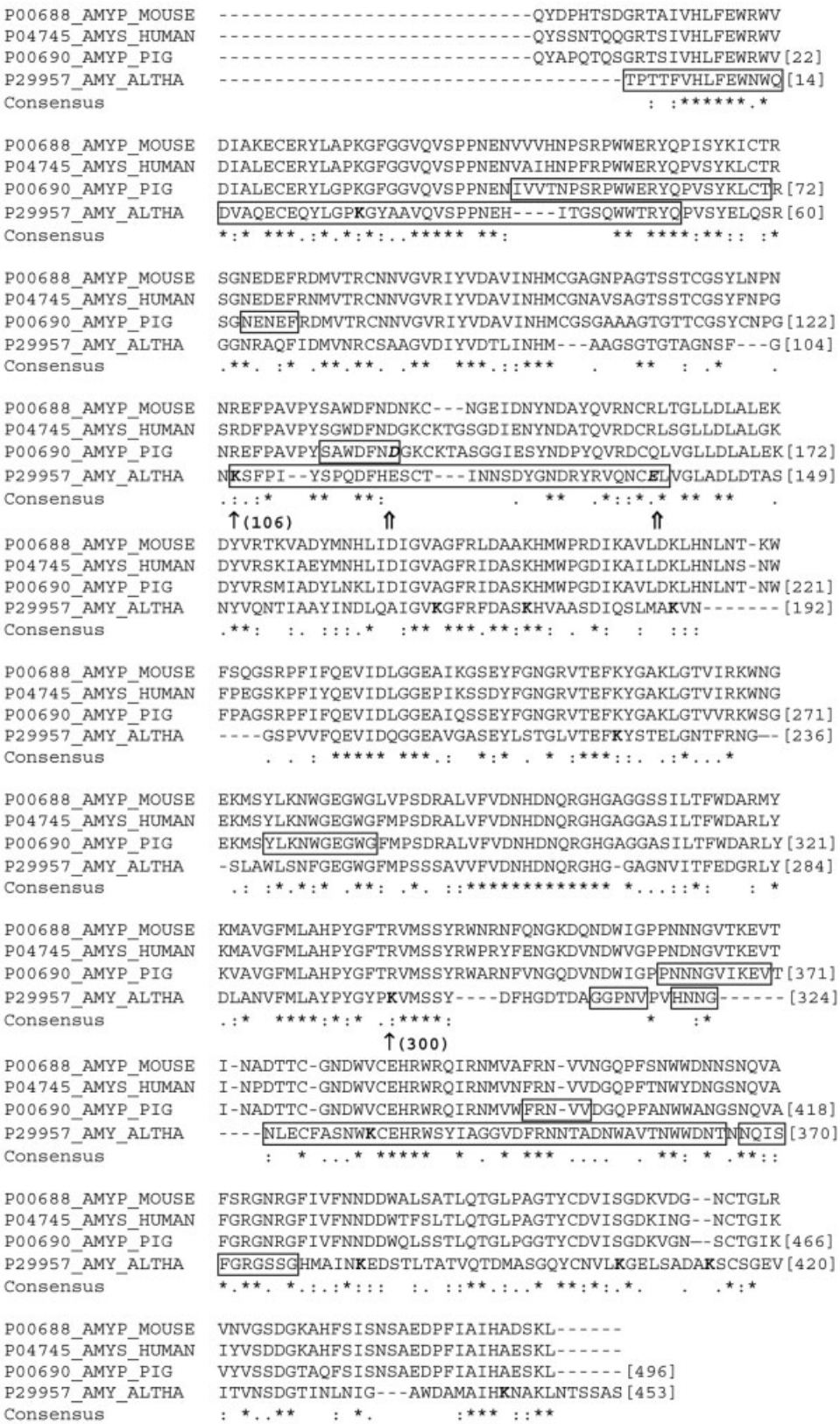
P00688_AMYP_MOUSE ----------QYDPHTSDGRTAIVHLFEWRWV
P04745_AMYS_HUMAN ----------QYSSNTQQGRTSIVHLFEWRWV
P00690_AMYP_PIG ----------QYAPQTQSGRTSIVHLFEWRWV[22]
P29957_AMY_ALTHA ----------TPTTFVHLFEWNWQ[14]
Consensus : :******.*
P00688_AMYP_MOUSE DIAKECERYLAPKGFGGVQVSPPNENVVVHNPSRPWWERYQPISYKICTR
P04745_AMYS_HUMAN DIALECERYLAPKGFGGVQVSPPNENVAIHNPFRPWWERYQPVSYKLCTR
P00690_AMYP_PIG DIALECERYLGPKGFGGVQVSPPNENIVVTNPSRPWWERYQPVSYKLCTR[72]
P29957_AMY_ALTHA DVAQECEQYLGPKGYAAVQVSPPNEH----ITGSQWWTRYQPVSYELQSR[60]
Consensus *:* ***.:*.*:*:..***** **: ** ****:**:: :*
P00688_AMYP_MOUSE SGNEDEFRDMVTRCNNVGVRIYVDAVINHMCGAGNPAGTSSTCGSYLNPN
P04745_AMYS_HUMAN SGNEDEFRNMVTRCNNVGVRIYVDAVINHMCGNAVSAGTSSTCGSYFNPG
P00690_AMYP_PIG SGNENEFRDMVTRCNNVGVRIYVDAVINHMCGSGAAAGTGTTCGSYCNPG[122]
P29957_AMY_ALTHA GGNRAQFIDMVNRCSAAGVDIYVDTLINHM---AAGSGTGTAGNSF---G[104]
Consensus .**. :* .**.**. .** ***.::*** . ** : .* .
P00688_AMYP_MOUSE NREFPAVPYSAWDFNDNKC---NGEIDNYNDAYQVRNCRLTGLLDLALEK
P04745_AMYS_HUMAN SRDFPAVPYSGWDFNDGKCKTGSGDIENYNDATQVRDCRLSGLLDLALGK
P00690_AMYP_PIG NREFPAVPYSAWDFNDGKCKTASGGIESYNDPYQVRDCQLVGLLDLALEK[172]
P29957_AMY_ALTHA NKSFPI--YSPQDFHESCT---INNSDYGNDRYRVQNCELVGLADLDTAS[149]
Consensus .:.:* ** **: . ** .*::*.* ** ** .
↑(106) ⇑ ⇑
P00688_AMYP_MOUSE DYVRTKVADYMNHLIDIGVAGFRLDAAKHMWPRDIKAVLDKLHNLNT-KW
P04745_AMYS_HUMAN DYVRSKIAEYMNHLIDIGVAGFRIDASKHMWPGDIKAILDKLHNLNS-NW
P00690_AMYP_PIG DYVRSMIADYLNKLIDIGVAGFRIDASKHMWPGDIKAVLDKLHNLNT-NW[221]
P29957_AMY_ALTHA NYVQNTIAAYINDLQAIGVKGFRFDASKHVAASDIQSLMAKVN-------[192]
Consensus .**: :. :::.* :** ***.**:**: . *: : :::
P00688_AMYP_MOUSE FSQGSRPFIFQEVIDLGGEAIKGSEYFGNGRVTEFKYGAKLGTVIRKWNG
P04745_AMYS_HUMAN FPEGSKPFIYQEVIDLGGEPIKSSDYFGNGRVTEFKYGAKLGTVIRKWNG
P00690_AMYP_PIG FPAGSRPFIFQEVIDLGGEAIQSSEYFGNGRVTEFKYGAKLGTVVRKWSG[271]
P29957_AMY_ALTHA ----GSPVVFQEVIDQGGEAVGASEYLSTGLVTEFKYSTELGNTFRNG--[236]
Consensus . . : ***** ***.: *:* . * :***::. .:*...*
P00688_AMYP_MOUSE EKMSYLKNWGEGWGLVPSDRALVFVDNHDNQRGHGAGGSSILTFWDARMY
P04745_AMYS_HUMAN EKMSYLKNWGEGWGFMPSDRALVFVDNHDNQRGHGAGGASILTFWDARLY
P00690_AMYP_PIG EKMSYLKNWGEGWGFMPSDRALVFVDNHDNQRGHGAGGASILTFWDARLY[321]
P29957_AMY_ALTHA -SLAWLSNFGEGWGFMPSSSAVVFVDNHDNQRGHG-GAGNVITFEDGRLY[284]
Consensus .: :*.*:* .**: .*. ::************** *...::*: : *
P00688_AMYP_MOUSE KMAVGFMLAHPYGFTRVMSSYRWNRNFQNGKDQNDWIGPPNNNGVTKEVT
P04745_AMYS_HUMAN KMAVGFMLAHPYGFTRVMSSYRWPRYFENGKDVNDWVGPPNDNGVTKEVT
P00690_AMYP_PIG KVAVGFMLAHPYGFTRVMSSYRWARNFVNGQDVNDWIGPPNNNGVIKEVT[371]
P29957_AMY_ALTHA DLANVFMLAYPYGYPKVMSSY----DFHGDTDAGGPNVPVHNNG------[324]
Consensus .:* ****:*:* .:****: * :*
↑(300)
P00688_AMYP_MOUSE I-NADTTC-GNDWVCEHRWRQIRNMVAFRN-VVNGQPFSNWWDNNSNQVA
P04745_AMYS_HUMAN I-NPDTTC-GNDWVCEHRWRQIRNMVNFRN-VVDGQPFTNWYDNGSNQVA
P00690_AMYP_PIG I-NADTTC-GNDWVCEHRWRQIRNMVWFRN-VVDGQPFANWWANGSNQVA[418]
P29957_AMY_ALTHA ----NLECFASNWKCEHRWSYIAGGVDFRNNTADNWAVTNWWDNTNNQIS[370]
Consensus : * ...* ***** * . * *** .... . **: * .**::
P00688_AMYP_MOUSE FSRGNRGFIVFNNDDWALSATLQTGLPAGTYCDVISGDKVDG--NCTGLR
P04745_AMYS_HUMAN FGRGNRGFIVFNNDDWTFSLTLQTGLPAGTYCDVISGDKING--NCTGIK
P00690_AMYP_PIG FGRGNRGFIVFNNDDWQLSSTLQTGLPGGTYCDVISGDKVGN--SCTGIK[466]
P29957_AMY_ALTHA FGRGSSGHMAINKEDSTLTATVQTDMASGQYCNVLKGELSADAKSCSGEV[420]
Consensus *.**. *.:.:*::: :. ::**.:..* **:*:.*. . .*:*
P00688_AMYP_MOUSE VNVGSDGKAHFSISNSAEDPFIAIHADSKL------
P04745_AMYS_HUMAN IYVSDDGKAHFSISNSAEDPFIAIHAESKL------
P00690_AMYP_PIG VYVSSDGTAQFSISNSAEDPFIAIHAESKL------[496]
P29957_AMY_ALTHA ITVNSDGTINLNIG---AWDAMAIHKNAKLNTSSAS[453]
Consensus : *..** : *. :*** ::**

Figure 8.

ing cooperativity of the hR-modified enzyme increases at low temperature (12°C; Fig. 4).

Performing TUG-GE under the same conditions but in the absence of Ca^{2+} showed fast, reversible unfolding for both the unmodified and modified enzyme (Fig. 5). This illustrates that Ca^{2+} is required to bring about slow unfolding under these conditions of electrophoresis.

In the presence of Ca^{2+} at pH 10.4, TUG-GE of modified AHA (17 h) did not show an obvious break in the curve describing the first transition (Fig. 4). It is possible that at high pH, Ca^{2+} forms $Ca(OH)_2$ and is sufficiently insoluble to exert the same effect that it does at more neutral pH.

The data presented in Figure 4 allows some conclusions to be made about the physical nature of the first transition for the modified enzyme in the presence of Ca^{2+}; that is, a transition that corresponds to a slow unfolding process. The observed break in the unfolding curve indicates that this is an all-or-none transition, and is an intramolecular analog of the macroscopic first-order phase transitions. The first stage of the urea-induced unfolding of the modified AHA in the presence of Ca^{2+} is a highly cooperative transition, which separates two conformations: a compact tightly folded native state and a less compact partially folded intermediate conformation. In other words, this partially folded conformation represents a definite phase state of the α-amylase. To some extent this resembles a multistate unfolding, globular protein with an accumulation of molten globule-like intermediates. It has previously been shown that the molten globule can be separated from native and unfolded conformations by first-order phase transitions.[66–69]

Effects of Guanidination on the Kinetics and Thermodynamics of Activity

The α-amylase activity of AHA decreased with increasing duration of guanidination. For example, at 25°C, k_{cat} decreased to 5%, 1%, and 0.5% after 17, 46, and 66 h guanidination, respectively (Table III). This decrease was accompanied by an increase in $\Delta H^{\#}$; at 3°C and 25°C, $\Delta H^{\#}$ of the modified enzyme (17 h) was 6 kJ mol^{-1} higher than the unmodified enzyme. The increase in $\Delta H^{\#}$ indicates that the decrease in activity is enthalpy driven. The T_{opt} of unmodified and modified AHA did not change significantly (Table III). As shown in many other studies,[5] decreasing the activity and/or thermolability of an enzyme does not necessarily produce an increased thermoactivity (T_{opt}). Guanidination for 17 and 46 h led to a decrease in K_m (Table III). When calculated from activity data at 25°C, K_m decreased from 2.9 mg mL^{-1}, to 1.3 mg mL^{-1} and 2.0 mg mL^{-1} for 17 h and 46 h of guanidination, respectively. A similar trend was observed for AHA modified for 17 h when calculated from activity data measured at 3°C. Guanidination for 66 h appeared to lead to an increase in K_m (Table III). However, the activity for this enzyme was very low and may compromise the accuracy of the extrapolations required to calculate the kinetic and thermodynamic data.

Far-UV Circular Dichroism Spectra

The TUG-GE and activity data are indicative of guanidination causing an increase in stability at the expense of activity. Far-UV CD has previously been used to examine the secondary structure of wild-type AHA compared to other more stable α-amylases (e.g., PPA).[12] The far-UV CD spectra of the unmodified AHA displayed a prominent minima near 222 nm, and a weak signal near 208 nm which may reflect weakly organized helical structures (Fig. 6); characteristics that have previously been reported for this enzyme.[12] The hR-modified AHA (17 h) displayed a stronger signal near 208 nm (Fig. 6), and is indicative of more organized helical structures.[12]

Proteolytic Nicking

Limited proteolytic digestion has previously been used to probe the compactness of a protein's tertiary structure.[50,51] To compare the structural flexibility of unmodified and hR-modified (17 h) AHA, chymotrypsin was used and the rate of degradation was monitored (Fig. 7). The relative decrease in band intensity was essentially identical for the modified and unmodified enzymes, indicating that guanidination had little effect on the overall tertiary structure of AHA (Fig. 7).

Modeling Changes in Protein Structure and Composition

The primary amino acid sequence of AHA was aligned with orthologs from mammals (including pig) to identify naturally occurring lysine to arginine replacements (Fig. 8). Out of 13 K residues in AHA, only two (K106 and K300) are replaced by R residues in the mammalian sequences (e.g., R124 and R337 in PPA; Fig. 8). In the crystal structure of the PPA (PDB: 1OSE), R124 forms a salt bridge with D138, and R337 is implicated in Cl^- binding.[70] The R124–D138 salt bridge is located in Domain B. The role that this salt bridge may play in enhancing rigidity of the active site has not been addressed. In contrast, the R337 residue has been suggested to decrease the strength of Cl^- binding due to bidentate coordination and reduce α-amylase activity of the mammalian enzymes; this compares to AHA in which K300 binds Cl^- via unidentate coordination.[10,71]

Overlaying hR on K106 in the crystal structure is suggestive that hR106 may form a salt bridge with E138 (Table IV, Fig. 9). Both residues, K106 and E138, have accessible surface areas of only 12.5% and 7.6%, respectively, illustrating that the crucial hR106–E138 salt bridge

Fig. 8. Sequence alignments and intrinsically unfolded regions of α-amylases. T-COFFEE and FoldIndex were used for constructing sequence alignments and determining intrinsically unfolded regions, respectively. α-Amylase sequences: mouse pancreatic, AMYP_MOUSE; PPA, AMYP_PIG; human salivary, AMYS_HUMAN; AHA, AMY_ALTHA. Numbers in square parentheses show residue number for AHA and PPA only. The conserved residues in all five α-amylases are shown on the consensus line. K residues in AHA, bold letters; K residues (AHA) replaced by R residues in the mammalian sequences, (↑); acidic residues, E138 in AHA and D138 in PPA are bold italic and marked (⇑); fully conserved amino acid residues, (*); residues with approximately the same size and hydropathy (:); residues with approximately the same size or hydropathy, (.); predicted disordered regions in AHA or PPA, open-boxed residues.

TABLE IV. Modeling of H Bonds and Salt Bridges Formed by the Side-Chains of hR Residues in the AHA X-Ray Structure[a]

Residue number	B-Factor (NE) Å[b]	H Bond (due to K)	Remarks	Salt Bridge (due to K)	Remarks
27	45	—	—	E408(monodentate), α/β barrel to Domain C	hR may alter salt-bridge to bidentate, but high B-factor indicates disorder
106	26	S117 (C═O) S119 (OH) Between S3 and H3 of α/β barrel (pins two halves of Domain B)	hR may improve weak h-bond to S119 (OH)	none	hR may make salt-bridge to E138
169	40	none	Solvent exposed, disordered	none	Solvent exposed, disordered
177	20	1202 (C═O) Stabilizes S5-H5 loop near active-site	No new interactions	E207	No new interactions
190	30	N150 & N154 Surface of H4-H3	No new interactions, High B-factor	none	—
224	19	G249 (C═O) S6-H in loop 6	No new interactions	none	—
300	12	Q33, $2H_2O$ & Cl^-	Cl^- displaced, too close to H263 & R172, damage active-site, alter activity	none	—
334	22	A330 (C═O)	hR could possibly make an extra H-bond to F329 (C═O), which may increase loop 8 stability	none	—
383	19	F233 (C═O)	hR could make an extra H-bond to R234 (C═O) Inter-domain A-C	none	—
406	25	none	—	D437 & E419 Link two halves of Domain C	No new interactions
414	−55	none	Exposed, disordered	none	Exposed, disordered
443	40	none	disordered	D354	No improvement
446	30	H_20 (weak)	hR may make H-bond to S398 (C═O) Intra-domain C, Near C-terminal	none	—

[a]The PDB number for AHA is 1AQM. Bold residues numbers indicate formation of electrostatic interactions in modified K (hR).

is not completely solvated. Such an additional intra-Domain B salt bridge could stabilize this part of the structure, which may lead to the slow unfolding observed at 12°C within the duration of TUG-GE (Fig. 4). Modeling K300hR indicates that no new interactions are likely to occur. However, a K300hR modification is likely to severely disrupt the active site, possibly displacing the Cl^- ion and a water molecule in the structure (Table IV, Fig. 9).

The modeling indicates that a few other changes are also possible. hR27 may alter salt-bridge formation from monodentate to become bidentate with E408, thereby locking the N-terminal part of Domain A to Domain C (Table IV). hR334 may form an additional H bond to F329 (C═O), and hR383 may form a H bond to R234 (Table IV).

The FoldIndex algorithm has been found to be a good predictor of disordered regions in proteins,[58] and was used to analyze the sequences of AHA and PPA (Fig. 8). FoldIndex predicted three main disordered regions in AHA (residues T1–H40 in Domain A, residues K106–L139 in Domain B, and residues N325–T365 comprising the C-terminal part of Domain A and N-terminal part of Domain C), which were not obviously disordered in PPA (boxed sequence, Fig. 8). All three regions that were predicted to be intrinsically disordered contained a K residue (K27, K106, and K334). When converted to hR, these may form additional electrostatic interactions (Table IV). Interestingly, the Domain B part of the active site (K106–L139) in AHA, which contains both K106 and E138, was predicted to be intrinsically disordered (Fig. 8).

Compositional profiling was performed with AHA, PPA, and α-amylases from human and mouse (Fig. 10), based on the approach developed for intrinsically disordered proteins.[23] The fractional difference in composition between an amino acid type in AHA and an equivalent amino acid type in the α-amylases from mesophiles (pig, human, and mouse), is depicted by bars in Figure 10. AHA has a reduced number of structure-promoting amino acids (Fig. 10, left side; e.g., W, F, C, and I) and an increased number

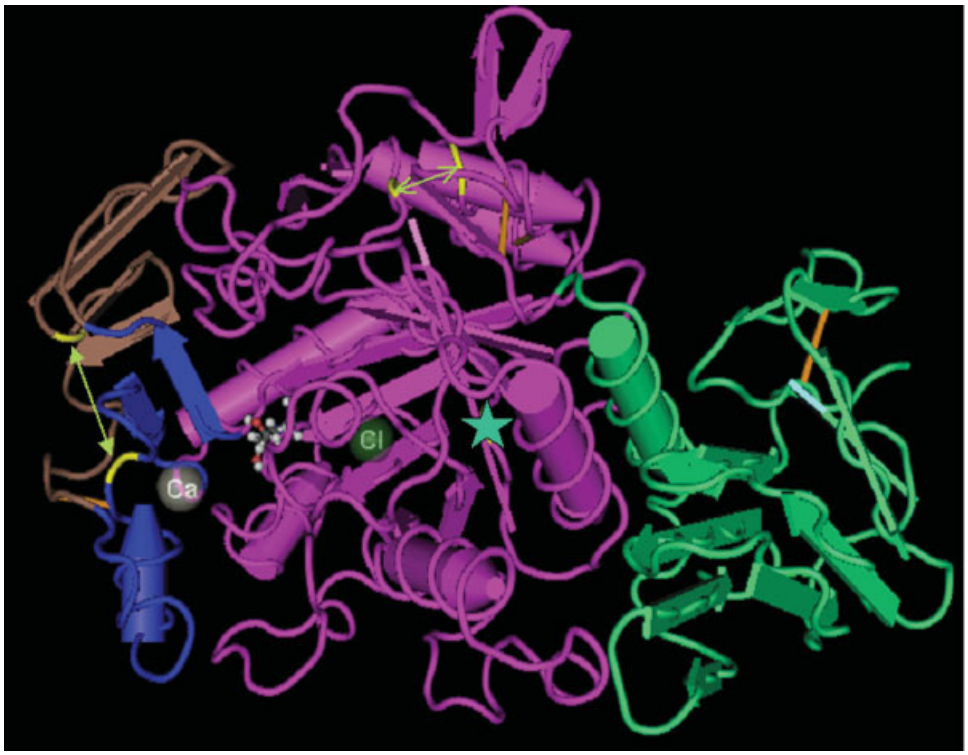

Fig. 9. Structure of α-amylase from *Pseudoalteromonas haloplanktis*. Important hR interactions are shown in a model based on the AHA (1AQM) crystal structure. Depicted in the model are α-helices, cylinders; β-stands, single arrows; random coils, wires connecting α-helices and β-stands; intra-Domain B salt bridge (hR106–E138), solid double-headed arrow; intra-Domain A salt bridge (R12–D15), open double-headed arrow; residues involved in hR106 to E138 and R12 to D15 salt bridges (yellow); disufide bridges (orange); K300hR modification (star) is shown in close proximity to a chloride ion (Cl); a calcium ion (Ca) is shown between central domain A (pink) and domain B (blue and brown); domain C (green).

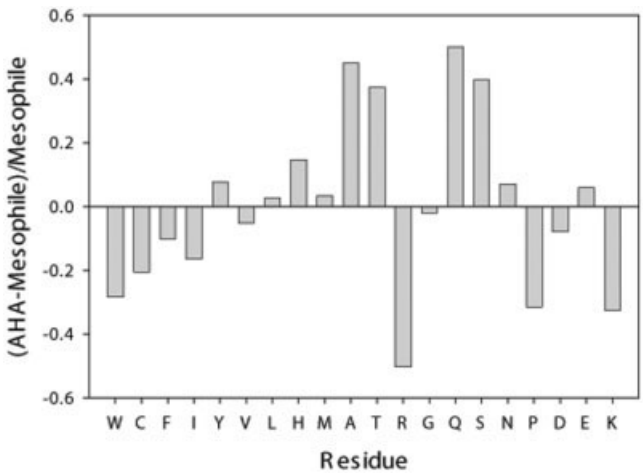

Fig. 10. Composition profiling of AHA. The bar for a given amino acid represents the fractional difference in composition between a residue-type from AHA and the same residue-type from a set of α-amylases from mesophiles (human, pig, and mouse). The fractional difference is calculated as $(C_{AHA} - C_{meso})/C_{meso}$, where C_{AHA} is the composition of a given amino acid in AHA, and C_{meso} is the corresponding composition in a set of α-amylases from mesophiles. The residues are ordered by Vihinen's flexibility scale.[76]

of specific, disorder-promoting amino acids (Fig. 10, right side; e.g., A, T, Q, and S). A reduction in the number of the bulky hydrophobic residues, W, F, and I, was observed and may lead to a weakening of hydrophobic interactions in the core of AHA. The decreased content of C-residues may also contribute to decreased protein conformational stability. The relatively low content of charged residues, R, D, and K, may also contribute to the decreased thermostability of AHA by decreasing the total number of ionic interactions.

Conformational Stability of an N12R Mutant that Forms an Intramolecular Salt Bridge within Domain A

To further probe the effect of introducing a salt bridge near the active site on the conformational stability of AHA, we examined the stability of an N12R site-directed mutant. The N12R replacement in the N-terminal part of Domain A produces an extra salt bridge with D15 that decreases thermal unfolding cooperativity of the enzyme (Fig. 9).[13] Using specific TUG-GE conditions, the N12R mutation was also shown to produce relatively slow unfolding of the structures corresponding to the first transition of the unfolding curve.[14] To examine the stability of the N12R mutant under conditions which promoted reversible unfolding, TUG-GE was performed at 30°C, pH 8.8 in the presence of Ca^{2+} (Fig. 11). The unfolding pattern of the mutant was similar to the unmodified (wild-type) enzyme demonstrating that under these conditions unfolding was fully reversible. The ΔG and $(urea)_{1/2}$ for the N12R mutant

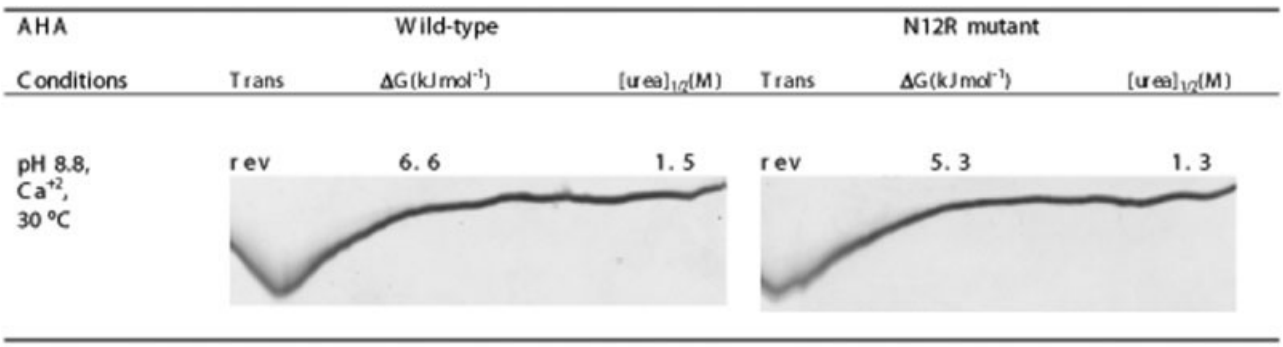

Fig. 11. Urea unfolding curves and thermodynamic parameters of wild-type and N12R AHA. TUG-GE performed at pH 8.8 in the presence of Ca^{2+} at 30°C. Urea gradient was 0 to 6.64*M* (left to right); direction of electrophoresis, top to bottom; Trans, folding/unfolding transition; rev, reversible transition; ΔG, free energy of unfolding between transitions; $(urea)_{1/2}$, urea concentration at 0 ΔG.

(5.3 kJ mol^{-1}, 1.3*M*) was slightly lower than the wild-type (6.6 kJ mol^{-1}, 1.5*M*), demonstrating that the mutant enzyme was marginally less stable (Fig. 11).

DISCUSSION

Our study provides new insight into the structure–function–stability relationship of cold-adapted AHA. Amongst the numerous structural features implicated in generating high flexibility in AHA and other cold-adapted proteins,[3,10,11] we show that K residues facilitate protein cold adaptation at the expense of R residues. This is the first experimental data using a cold-adapted enzyme that supports the trends that have been predicted from compositional, modeling, and structural studies.[2] We also identified a K residue in the active site of AHA that plays important roles in ensuring that the active site retains local flexibility, and is the least stable structure in the enzyme. An additional lysine was linked to Cl^- ion binding and maintaining enzyme activity. Our study more broadly demonstrated that chemical modification is useful for providing detailed knowledge of structure–function–stability, and therefore holds potential for guiding future targeted studies of specific structural features, including an attempt to convert a mesophilic α-amylase into a cold-adapted enzyme.

Understanding AHA Flexibility from Computational Analysis of the Amino Acid Sequence

Natively unfolded (intrinsically disordered) proteins possess a very high level of intramolecular flexibility under physiological conditions. They exist as dynamic ensembles in which atom positions and backbone Ramachandran angles vary significantly over time with no specific equilibrium values, and they typically undergo noncooperative conformational changes. In contrast, ordered proteins are relatively stable and Ramachandran angles vary slightly around their equilibrium positions, and exhibit occasional cooperative conformational switching. Intrinsically disordered proteins have a number of structural and compositional features that distinguish them from ordered proteins.[23,30,31] Consistent with the features of intrinsically disordered proteins, a plot of the mean net charge versus mean hydrophobicity of AHA showed that the N- and C-terminal parts of Domain A and active-site region of Domain B, are more flexible than in PPA (Fig. 8). The amino acid composition of AHA is also somewhat depleted in the major order-promoting (C, W, F, and I) and enriched in several disorder-promoting amino acids (A, T, S, and Q), has a relatively low number of bulky hydrophobic residues which might weaken hydrophobic interactions, and a relatively low content of charged residues, R, D, and K, which might decrease the total number of ionic interactions. These characteristics of AHA amino acid composition are likely to reflect a requirement for proper solvation of the enzyme at low temperatures. Proper solvation is achieved by the relaxation of the AHA structure, which is driven by the compositional bias that favors decreased conformational stability and increased flexibility. Interestingly, these cold adaptation–related biases in amino acid composition resemble those described for intrinsically disordered proteins.

Factors Determining the Efficiency of Guanidination

It may be expected that the sites of most effective guanidination would be located in regions predicted to be more flexible and highly solvent exposed. While none of the K residues were highly exposed to the solvent on the protein's surface, the reactivity of lysine residues could not be linked to solvent accessibility, steric hindrance, or predisposition to disorder (Fig. 2). These data may indicate that the rate of modification is determined by features of the protein surface in close proximity to each K residue. It is also possible that the ion composition in the chemical modification reactions has effected the hydration state of the enzyme[72] in ways that we have not been able to predict.

Importance of Lysine in Limiting Salt-Bridge Formation and Promoting Local Flexibility in the Active Site

Modifying lysine to hR produced a conformationally more stable enzyme. The increased stability is likely to relate to additional ionic interactions afforded by the hR side-chain.[15,42] The ionic interactions not only stabilized the overall structure, but produced localized effects. The unfolding of the domain undergoing first transition be-

came slow (slower than the duration of TUG-GE) due to the increased cooperativity of unfolding (Fig. 4).

Unfolding cooperativity in AHA has been linked to a requirement for a small number of interactions to preserve the native state.[13,73] Under conditions that promote unfolding, noncovalent interactions would be rapidly disrupted resulting in two-state unfolding. In mammals, R replaces K at position 106 in AHA (Fig. 8). The equivalent R residue (R124 in PPA) forms a salt bridge with D138 that locks the Domain B part of the active site, and is likely to contribute to the higher stability and slow unfolding of this enzyme.[70] It is also notable that R124 to D138 is the sole intradomain B salt bridge found in PPA.[70] In modified AHA, hR106 may facilitate an equivalent salt bridge with E138 and stabilize the part of Domain B which is in the active site (Fig. 9). The ion pair in modified AHA (hR106–E138) and PPA (R124–D138) bridges a region more than 10 residues apart, and may be considered a critical ion pair.[74] As K106 in unmodified AHA is unable to form an equivalent ion pair, it may be particularly important for promoting a high level of active-site flexibility. Other guanidinated K residues such as hR27, hR334, and hR383 may also contribute to stabilization through salt-bridge and/or H-bonding interactions (Table IV).

Under conditions that enabled reversible unfolding to occur, the N12R mutant was found to be marginally less stable than unmodified AHA (Fig. 11). This indicates that the R12 to D15 intra-Domain A salt bridge has little effect on the overall conformational stability of AHA. This may be due to the solvation penalty involved in forming a salt bridge between the side-chains of arginine and aspartate,[75] and/or that R12 to D15 bridges a short segment (3 amino acids) at the N-terminal end of the enzyme (Fig. 9).[74] If the conformational stability of the modified enzyme is largely due to the hR106 to E138 intra-Domain B salt bridge (see above), it would indicate that the lack of K106 to E138 salt bridge is more important for cold adaptation of AHA than the lack of a R12 to D15 salt bridge.

Comparative analyses of the X-ray structures of AHA and PPA have previously identified ~ 30 conserved side-chains in and around the active-site region.[1,10] Due to the high level of similarity, it was proposed that structural adaptations away from the active site were important for the high flexibility of AHA, and that the enzyme may be uniformly unstable throughout most of its structure.[1,12,38] A subsequent study using TUG-GE revealed that the most flexible region in AHA is around the active site.[14] In combination with the previous study,[14] our present work demonstrates that parts of Domains A and B that are in the active site form a region of local flexibility that unfolds first in the unfolding pathway.

Low Activity Is Enthalpy Driven

The k_{cat} of the modified enzyme decreased with a concomitant increase in $\Delta H^{\#}$ and decrease in K_m (Table III). These changes broadly reflect structural changes associated with more thermally stable enzymes from mesophiles (e.g., PPA). A reduction in $\Delta H^{\#}$ is achieved by decreasing the number of enthalpy-driven interactions that have to be broken during formation of the transition state. These interactions also contribute to the stability of the folded conformation and therefore the domain of the enzyme bearing the active site is necessarily less stable. This enthalpy effect is the prime reason for the activity-stability trade-off associated with cold-adapted enzymes.[2,38,73] This indicates that hR modification produces more enthalpy-driven interactions than in the unmodified enzyme. This may be explained by hR residues forming multiple ionic interactions and creating a more rigid enzyme with reduced activity.

The decreased k_{cat} of the modified enzyme was also accompanied by a decrease in K_m (Table III). Previous site-directed mutagenesis studies identified a similar trend with both k_{cat} and K_m decreasing.[13,40] A higher level of flexibility may lead to a wider distribution of enzyme conformations and hence a higher K_m. Increasing the number of ionic interactions, particularly near the active site, will increase rigidity and hence decrease k_{cat} and K_m.[13] In the hR-modified enzyme, this increase in rigidity may be explained by a hR106 to E138 salt bridge in Domain B.

Role of Ca^{2+} and Cl^- in the Active Site

In the modified (17 h) enzyme, the first transition became slow only when TUG-GE (pH 7.5 and 8.8) was performed in the presence of Ca^{2+} (Fig. 4). AHA has ~ 3000-fold lower affinity for Ca^{2+} than PPA, and is proposed to be an important factor contributing to cold activity.[10] Ca^{2+} was previously found to stabilize the structures corresponding to the first transition, and to have little effect on the second transition.[14] Moreover, it was shown that the N12R mutant underwent slow unfolding only in the presence of Ca^{2+}.[14] Our data is therefore consistent with Ca^{2+} binding between Domains A and B (Fig. 9), providing sufficient stability to the flexible active site to ensure activity is maintained in the cold.

Modifying K to hR produced a conformationally more stable, but less active α-amylase. A 95% and 99% reduction in activity occurred following 17 and 46 h of modification, respectively (Table III). The large reduction in activity relative to the gain in stability indicates that the loss in activity is not solely due to increased rigidity of the enzyme, as would be predicted purely from a trade-off in activity-stability. The loss in activity (Table III) was mirrored by the extent of modification of K300 (Tables I, II). MALDI-TOF-MS revealed that K300 is one of the most reactive K residues in AHA; 95% guanidination occurred after 17 h in contrast to 34% to 89% for other K residues examined. AHA, and other α-amylases in this family require Cl^- as an allosteric effector for their high activity, and K300 is known to be essential for its coordination.[10,71] In less active mammalian α-amylases, K300 is replaced by an R residue (Fig. 8). A K300R site-directed mutant of AHA exhibited an increased K_d of 10-fold[71] and a 50% decrease in $k_{cat,}$ compared to the wild type.[13] The decrease in Cl^- affinity was interpreted to be due to the presence of a more bulky guanidinium group.[71] The extra CH_2 in hR (1.54 Å) is predicted to cause Cl^- displacement due to its

close proximity to H263 and R172 (Table IV). Our data therefore suggests that in addition to reducing salt-bridge formation in the active site, K residues (rather than R residues) are important for maintaining effective Cl^- ion binding.

CONCLUSION

The Domain B part of the active site is predicted to be flexible, and a hR106 to E138 salt bridge appears to promote enhanced stability of this region. Due to the important roles inferred for K106 and K300, it will be challenging, but very valuable to determine a strategy for preserving K300 while guanidinating other K residues, in order to further our understanding of their role in the structure–activity–stability relationship of AHA. Clearly, it will also be useful to adopt the approach we have taken (e.g., chemical modification) to globally study the role of K residues in other cold-adapted enzymes.

ACKNOWLEDGMENTS

We are grateful to Andrew Mynott for help in CD spectrometry, and to Marilyn Katrib for editorial assistance. S. D'Amico is a postdoctoral researcher from the Fonds National de la Recherche Scientifique (FNRS, Belgium). Mass spectrometric analysis for the work were carried out at the Bioanalytical Mass Spectrometry Facility, UNSW, and was supported in part by grants from the Australian Government Systemic Infrastructure Initiative and Major National Research Facilities Program (UNSW node of the Australian Proteome Analysis Facility) and by the UNSW Capital Grants Scheme.

REFERENCES

1. Feller G, Gerday C. Psychrophilic enzymes: hot topics in cold adaptation. Nat Rev Microbiol 2003;1:200–208.
2. Feller G. Molecular adaptations to cold in psychrophilic enzymes. Cell Mol Life Sci 2003;60:648–662.
3. Cavicchioli R, Siddiqui KS. Cold-adapted enzymes. In: Pandey A, Webb C, Soccol CR, Larroche C, editors. Enzyme technology. New Dehli: AsiaTech Publishers; 2004. p 615–638.
4. D'Amico S, Claverie P, Collins T, Georlette D, Gratia E, Hoyoux A, Meuwis MA, Feller G, Gerday C. Molecular basis of cold adaptation. Philos Trans R Soc Lond B Biol Sci 2002;357:917–925.
5. Siddiqui KS, Cavicchioli R. Cold adapted enzymes. Annu Rev Biochem 2006;75:403–433.
6. Margesin R, Schinner F. Cold-adapted organisms — ecology, physiology, enzymology and molecular biology. Berlin: Springer-Verlag; 1999. 416 p.
7. Margesin R, Schinner F. Biotechnological applications of cold-adapted organisms. Berlin: Springer-Verlag; 1999. 338 p.
8. Gerday C, Aittaleb M, Bentahir M, Chessa JP, Claverie P, Collins T, D'Amico S, Dumont J, Garsoux G, Georlette D, Hoyoux A, Lonhienne T, Meuwis MA, Feller G. Cold-adapted enzymes: from fundamentals to biotechnology. Trends Biotechnol 2000;18:103–107.
9. Cavicchioli R, Siddiqui KS, Andrews D, Sowers KR. Low-temperature extremophiles and their applications. Curr Opin Biotechnol 2002;13:253–261.
10. Aghajari N, Feller G, Gerday C, Haser R. Crystal structures of the psychrophilic alpha-amylase from *Alteromonas haloplanctis* in its native form and complexed with an inhibitor. Protein Sci 1998;7:564–572.
11. Smalas AO, Leiros HK, Os V, Willassen NP. Cold adapted enzymes. Biotechnol Annu Rev 2000;6:1–57.
12. Feller G, d'Amico D, Gerday C. Thermodynamic stability of a cold-active alpha-amylase from the Antarctic bacterium *Alteromonas haloplanctis*. Biochemistry 1999;38:4613–4619.
13. D'Amico S, Gerday C, Feller G. Structural determinants of cold adaptation and stability in a large protein. J Biol Chem 2001;276:25791–25796.
14. Siddiqui KS, Feller G, D'Amico S, Gerday C, Giaquinto L, Cavicchioli R. The active site is the least stable structure in the unfolding pathway of a multi-domain cold-adapted alpha-amylase. J Bacteriol 2005;187:6197–6205.
15. Feller G, Payan F, Theys F, Qian M, Haser R, Gerday C. Stability and structural analysis of alpha-amylase from the antarctic psychrophile *Alteromonas haloplanctis* A23. Eur J Biochem 1994;222:441–447.
16. Fields PA. Review: protein function at thermal extremes: balancing stability and flexibility. Comp Biochem Physiol A Mol Integr Physiol 2001;129:417–431.
17. Zecchinon L, Claverie P, Collins T, D'Amico S, Delille D, Feller G, Georlette D, Gratia E, Hoyoux A, Meuwis MA, Sonan G, Gerday C. Did psychrophilic enzymes really win the challenge? Extremophiles 2001;5:313–321.
18. Beadle BM, Shoichet BK. Structural bases of stability-function tradeoffs in enzymes. J Mol Biol 2002;321:285–296.
19. Zavodszky P, Kardos J, Svingor, Petsko GA. Adjustment of conformational flexibility is a key event in the thermal adaptation of proteins. Proc Natl Acad Sci U S A 1998;95:7406–7411.
20. Jaenicke R. Stability and stabilization of globular proteins in solution. J Biotechnol 2000;79:193–203.
21. Wright PE, Dyson HJ. Intrinsically unstructured proteins: reassessing the protein structure-function paradigm. J Mol Biol 1999;293:321–331.
22. Demchenko AP. Recognition between flexible protein molecules: induced and assisted folding. J Mol Recognit 2001;14:42–61.
23. Dunker AK, Lawson JD, Brown CJ, Williams RM, Romero P, Oh JS, Oldfield CJ, Campen AM, Ratliff CM, Hipps KW, Ausio J, Nissen MS, Reeves R, Kang C, Kissinger CR, Bailey RW, Griswold MD, Chiu W, Garner EC, Obradovic Z. Intrinsically disordered protein. J Mol Graph Model 2001;19:26–59.
24. Namba K. Roles of partly unfolded conformations in macromolecular self-assembly. Genes Cells 2001;6:1–12.
25. Dunker AK, Brown CJ, Lawson JD, Iakoucheva LM, Obradovic Z. Intrinsic disorder and protein function. Biochemistry 2002;41:6573–6582.
26. Uversky VN. Natively unfolded proteins: a point where biology waits for physics. Protein Sci 2002;11:739–756.
27. Gunasekaran K, Tsai CJ, Kumar S, Zanuy D, Nussinov R. Extended disordered proteins: targeting function with less scaffold. Trends Biochem Sci 2003;28:81–85.
28. Uversky VN, Oldfield CJ, Dunker AK. Showing your ID: intrinsic disorder as an ID for recognition, regulation and cell signaling. J Mol Recognit 2005;18:343–384.
29. Dyson HJ, Wright PE. Intrinsically unstructured proteins and their functions. Nat Rev Mol Cell Biol 2005;6:197–208.
30. Romero P, Obradovic Z, Dunker AK. Sequence data analysis for long disordered regions prediction in the calcineurin family. Genome Informatics 1997;8:110–124.
31. Dunker AK, Garner E, Guilliot S, Romero P, Albrecht K, Hart J, Obradovic Z, Kissinger C, Villafranca JE. Protein disorder and the evolution of molecular recognition: theory, predictions and observations. Pac Symp Biocomput 1998:473–484.
32. Romero P, Obradovic Z, Li X, Garner EC, Brown CJ, Dunker AK. Sequence complexity of disordered protein. Proteins 2001;42:38–48.
33. Vucetic S, Brown CJ, Dunker AK, Obradovic Z. Flavors of protein disorder. Proteins 2003;52:573–584.
34. Romero P, Obradovic Z, Kissinger CR, Villafranca JE, Dunker AK. Identifying disordered regions in proteins from amino acid sequences. Proc IEEE Int Conf Neural Networks 1997;1:90–95.
35. Li X, Romero P, Rani M, Dunker AK, Obradovic Z. Predicting protein disorder for N-, C-, and internal regions. Genome Inform Ser Workshop Genome Inform 1999;10:30–40.
36. Bracken C, Iakoucheva LM, Romero PR, Dunker AK. Combining prediction, computation and experiment for the characterization of protein disorder. Curr Opin Struct Biol 2004;14:570–576.
37. Violot S, Aghajari N, Czjzek M, Feller G, Sonan GK, Gouet P, Gerday C, Haser R, Receveur-Brechot V. Structure of a full length psychrophilic cellulase from *Pseudoalteromonas haloplanktis* revealed by X-ray diffraction and small angle X-ray scattering. J Mol Biol 2005;348:1211–1224.
38. D'Amico S, Gerday C, Feller G. Temperature adaptation of

proteins: engineering mesophilic-like activity and stability in a cold-adapted alpha-amylase. J Mol Biol 2003;332:981–988.
39. Siddiqui KS, Poljak A, Guilhaus M, Feller G, D'Amico S, Gerday C, Cavicchioli R. The role of disulfide-bridges in the activity and stability of cold-active alpha-amylase. J Bacteriol 2005;187:6206–6212.
40. D'Amico S, Gerday C, Feller G. Dual effects of an extra disulfide bond on the activity and stability of a cold-adapted alpha-amylase. J Biol Chem 2002;277:46110–46115.
41. Cupo P, El-Deiry W, Whitney PL, Awad WM Jr. Stabilization of proteins by guanidination. J Biol Chem 1980;255:10828–10833.
42. Mrabet NT, Van den Broeck A, Van den brande I, Stanssens P, Laroche Y, Lambeir AM, Matthijssens G, Jenkins J, Chiadmi M, van Tilbeurgh H, Rey F, Janin J, Quax WJ, Lasters I, DeMaeyer M, Wodak SJ. Arginine residues as stabilizing elements in proteins. Biochemistry 1992;31:2239–2253.
43. Feller G, Zekhnini Z, Lamotte-Brasseur J, Gerday C. Enzymes from cold-adapted microorganisms. The class C beta-lactamase from the antarctic psychrophile *Psychrobacter immobilis* A5. Eur J Biochem 1997;244:186–191.
44. Saunders NF, Thomas T, Curmi PM, Mattick JS, Kuczek E, Slade R, Davis J, Franzmann PD, Boone D, Rusterholtz K, Feldman R, Gates C, Bench S, Sowers K, Kadner K, Aerts A, Dehal P, Detter C, Glavina T, Lucas S, Richardson P, Larimer F, Hauser L, Land M, Cavicchioli R. Mechanisms of thermal adaptation revealed from the genomes of the Antarctic Archaea *Methanogenium frigidum* and *Methanococcoides burtonii*. Genome Res 2003;13:1580–1588.
45. Chessa JP, Feller G, Gerday C. Purification and characterization of the heat-labile alpha-amylase secreted by the psychrophilic bacterium TAC 240B. Can J Microbiol 1999;45:452–457.
46. Kruger NJ. The Bradford method for protein quantification. In: Walker JM, editor. The protein protocols handbook. Totowa, NJ: Humana Press; 2002. p 15–21.
47. Habeeb AFSA. Guanidination of proteins. Methods Enzymol 1972;25:558–566.
48. Siddiqui KS, Cavicchioli R, Thomas T. Thermodynamic activation properties of elongation factor 2 (EF-2) proteins from psychrotolerant and thermophilic Archaea. Extremophiles 2002;6:143–150.
49. Cavicchioli R, Curmi PM, Siddiqui KS, Thomas T. Proteins from psychrophiles. In: Rainey FA, Oren A, editors. Extremophiles — methods in microbiology, vol. 35. London: Elsevier; 2006. p. 395–436.
50. Siddiqui KS, Rangarajan M, Hartley BS, Kitmitto A, Panico M, Blench IP, Morris HR. Arthrobacter D-xylose isomerase: partial proteolysis with thermolysin. Biochem J 1993;289:201–208.
51. Watanabe S, Yasutake Y, Tanaka I, Takada Y. Elucidation of stability determinants of cold-adapted monomeric isocitrate dehydrogenase from a psychrophilic bacterium, *Colwellia maris*, by construction of chimeric enzymes. Microbiology 2005;151:1083–1094.
52. See YP, Jackowski G. Estimating molecular weights of polypeptides by SDS gel electrophoresis. In: Creighton TE, editor. Protein structure: a practical approach. Oxford: IRL Press; 1989. p 1–21.
53. Simpson RJ. Proteins and proteomics, a laboratory manual. Cold Spring Harbor, NY: Cold Spring Harbor Press; 2003.
54. Beavis R. PAWS-freeware computer program, edition for Windows NT. ProteoMetrics: 1998–2000. Available online at http://bioinformatics.genomicsolutions.com.
55. Poljak A, McLean CA, Sachdev P, Brodaty H, Smythe GA. Quantification of hemorphins in Alzheimer's disease brains. J Neurosci Res 2004;75:704–714.
56. Jones TA, Zou JY, Cowan SW, Kjeldgaard. Improved methods for building protein models in electron density maps and the location of errors in these models. Acta Crystallogr A 1991;47:110–119.
57. Notredame C, Higgins DG, Heringa J. T. Coffee: a novel method for fast and accurate multiple sequence alignment. J Mol Biol 2000;302:205–217.
58. Prilusky J, Felder CE, Zeev-Ben-Mordehai T, Rydberg EH, Man O, Beckmann JS, Silman I, Sussman JL. FoldIndex: a simple tool to predict whether a given protein sequence is intrinsically unfolded. Bioinformatics 2005;21:3435–3438.
59. Uversky VN, Gillespie JR, Fink AL. Why are natively unfolded proteins unstructured under physiologic conditions? Proteins 2000;41:415–427.
60. Fontana A, Polverino de Laureto P, De Filippis V, Scaramella E, Zambonin M. Probing the partly folded states of proteins by limited proteolysis. Fold Des 1997;2:R17–R26.
61. Fontana A, de Laureto PP, Spolaore B, Frare E, Picotti P, Zambonin M. Probing protein structure by limited proteolysis. Acta Biochim Pol 2004;51:299–321.
62. Iakoucheva LM, Kimzey AL, Masselon CD, Bruce JE, Garner EC, Brown CJ, Dunker AK, Smith RD, Ackerman EJ. Identification of intrinsic order and disorder in the DNA repair protein XPA. Protein Sci 2001;10:560–571.
63. Sobolev V, Sorokine A, Prilusky J, Abola EE, Edelman M. Automated analysis of interatomic contacts in proteins. Bioinformatics 1999;15:327–332.
64. Goldenberg DP, Creighton TE. Gel electrophoresis in studies of protein conformation and folding. Anal Biochem 1984;138:1–18.
65. Goldenberg DP. Analysis of protein conformation by gel electrophoresis. In: Creighton TE, editor. Protein structure: a practical approach. Oxford: IRL Press; 1989. p 225–250.
66. Uversky VN, Semisotnov GV, Pain RH, Ptitsyn OB. All-or-none mechanism of the molten globule unfolding. FEBS Lett 1992;314:89–92.
67. Uverskii VN, Semisotnov GV, Ptitsyn OB. [Molten globule unfolding by strong denaturing agents occurs by the all or nothing principle]. Biofizika 1993;38:37–46.
68. Ptitsyn OB, Uversky VN. The molten globule is a third thermodynamical state of protein molecules. FEBS Lett 1994;341:15–18.
69. Uversky VN, Ptitsyn OB. All-or-none solvent-induced transitions between native, molten globule and unfolded states in globular proteins. Fold Des 1996;1:117–122.
70. Qian M, Haser R, Payan F. Structure and molecular model refinement of pig pancreatic alpha-amylase at 2.1 A resolution. J Mol Biol 1993;231:785–799.
71. Feller G, Le Bussy O, Houssier C, Gerday C. Structural and functional aspects of chloride binding to *Alteromonas haloplanctis* alpha-amylase. J Biol Chem 1996;271:23836–23841.
72. Collins KD. Ions from the Hofmeister series and osmolytes: effects on proteins in solution and in the crystallization process. Methods 2004;34:300–311.
73. D'Amico S, Marx JC, Gerday C, Feller G. Activity-stability relationships in extremophilic enzymes. J Biol Chem 2003;278:7891–7896.
74. Bae E, Phillips GN Jr. Structures and analysis of highly homologous psychrophilic, mesophilic, and thermophilic adenylate kinases. J Biol Chem 2004;279:28202–28208.
75. Strop P, Mayo SL. Contribution of surface salt bridges to protein stability. Biochemistry 2000;39:1251–1255.
76. Vihinen M. Relationship of protein flexibility to thermostability. Protein Eng 1987;1:477–480.